Electronic Supplementary Material (ESI) for Journal of Materials Chemistry C.

Supporting Information

Design of high-performance circularly polarized multiple resonance-based TADF materials via participatory chiral perturbation

Ping Li, Wenjing Li, Qixin Lv, Runfeng Chen, and Chao Zheng**

State Key Laboratory of Organic Electronics andInformation Displays & Institute of Advanced Materials (IAM), Nanjing University of Posts &Telecommunications, Nanjing 210023, China

Contents

Figure S1. Calculated frontier orbital distributions of the investigated five different chiral units.

Figure S2. Diagram of geometry variations and calculated RMSD values between S_0 and S_1 states for the investigated molecules.

Figure S3. Optimized ground-state structures of model molecules.

Figure S4. Charge density differences of the investigated molecules.

Figure S5. Calculated Huang-Rhys factors versus the normal mode frequencies for the model, OBN, BN, BAM, CAI and PhCAI series molecules.

Figure S6. Sketch of the potential energy surfaces of the S_0 and S_1 of the investigated molecules.

Figure S7. Experimental circular dichroic spectrum for *p*-BN-OBN and simulated electronic circular dichroism spectra for OBN, BNA, BAM, CAI and PhCAI series molecules.

Figure S8. Changing trends between the chiral participations in HOMO composition and the g_{PL} values of different chiral series.

Figure S9. Calculated vertical excitation energies for OBN, BN, CAI and PhCAI series molecules in toluene.

Table S1. Absorption wavelength calculated by different functional for *p*-OBN.

Table S2. Calculated the maximum absorption and emission wavelengths, transition characters, FWHM values and reorganization energies of the investigated molecules.

Table S3. Calculated percentage of different molecular segments in HOMO composition and the g_{PL} values.

Table S4. Calculated oscillator strengths and radiation rates of the investigated molecules.

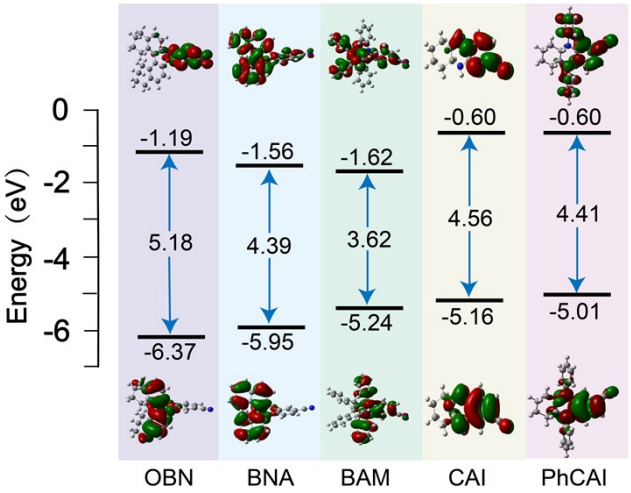

Figure S1. Calculated HOMO and LUMO energy levels and frontier orbital distributions of the investigated chiral units.

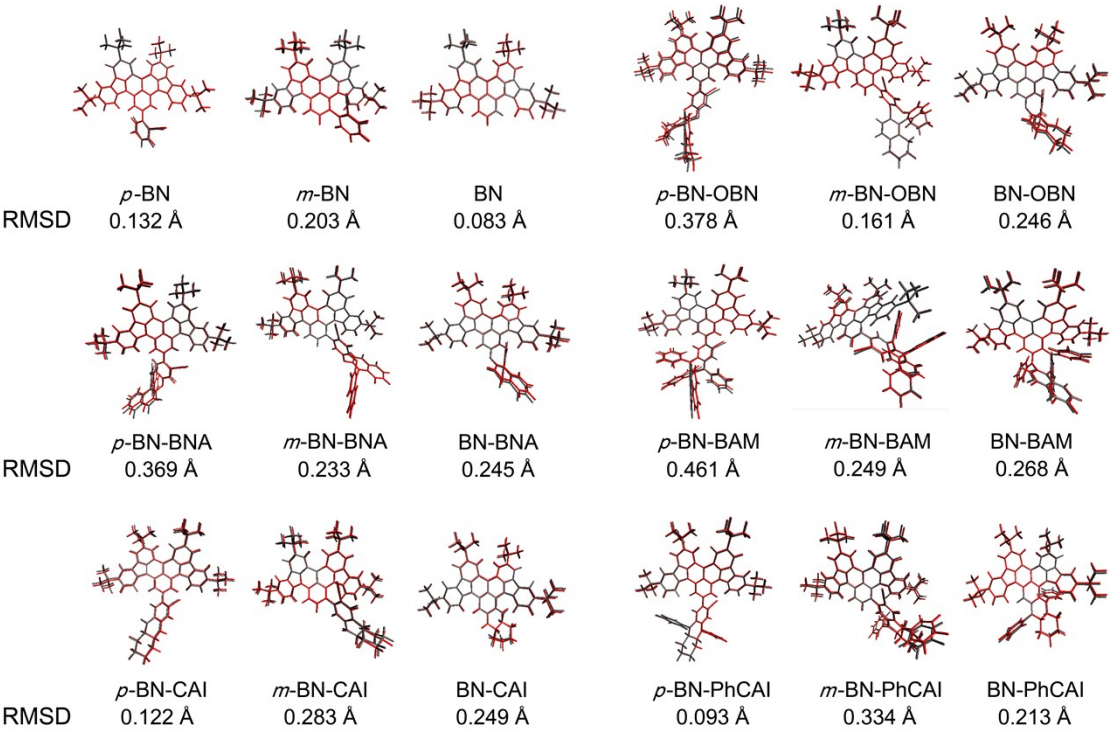

Figure S2. Diagram of geometry variations and calculated RMSD values between S_0 and S_1 states of the investigated molecules (The structures at S_0 and S_1 state are depicted in gray and red, respectively).

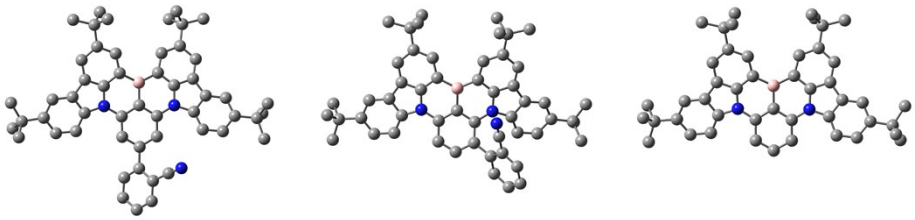

Figure S3. Optimized ground-state structures of model molecules (Saturated H atoms are not shown).

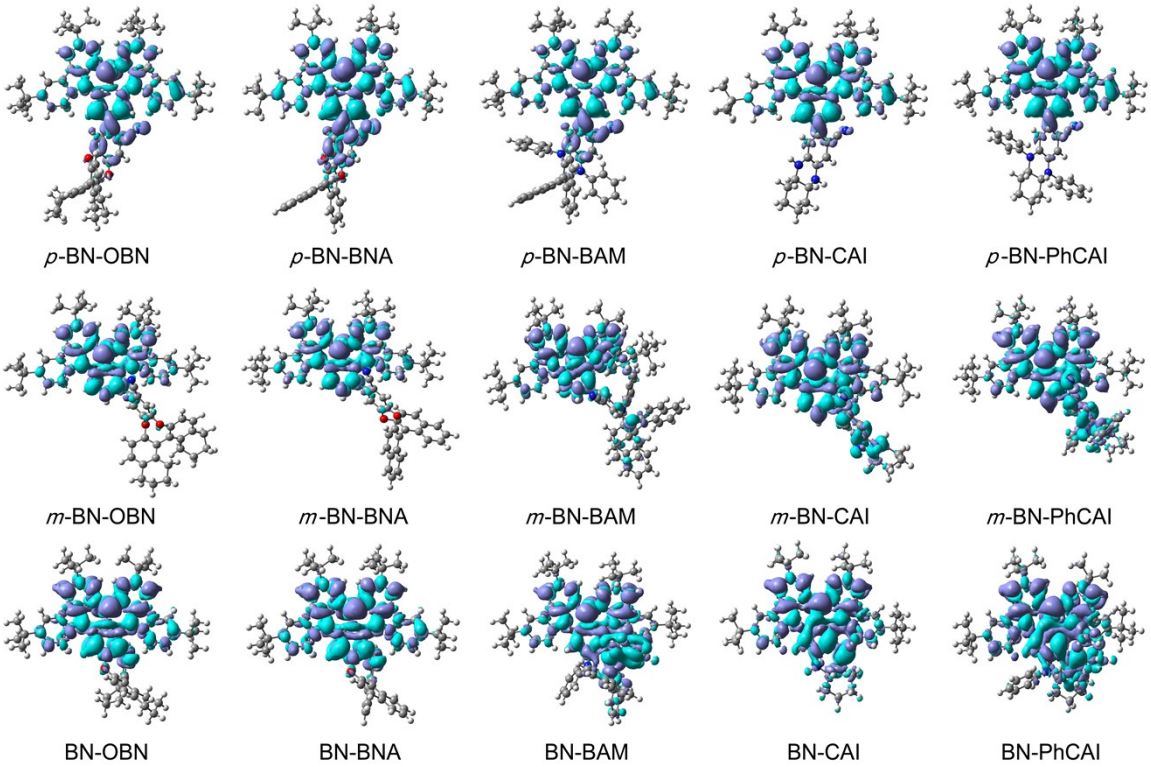

Figure S4. Charge density differences between the S_1 and S_0 of the investigated molecules.

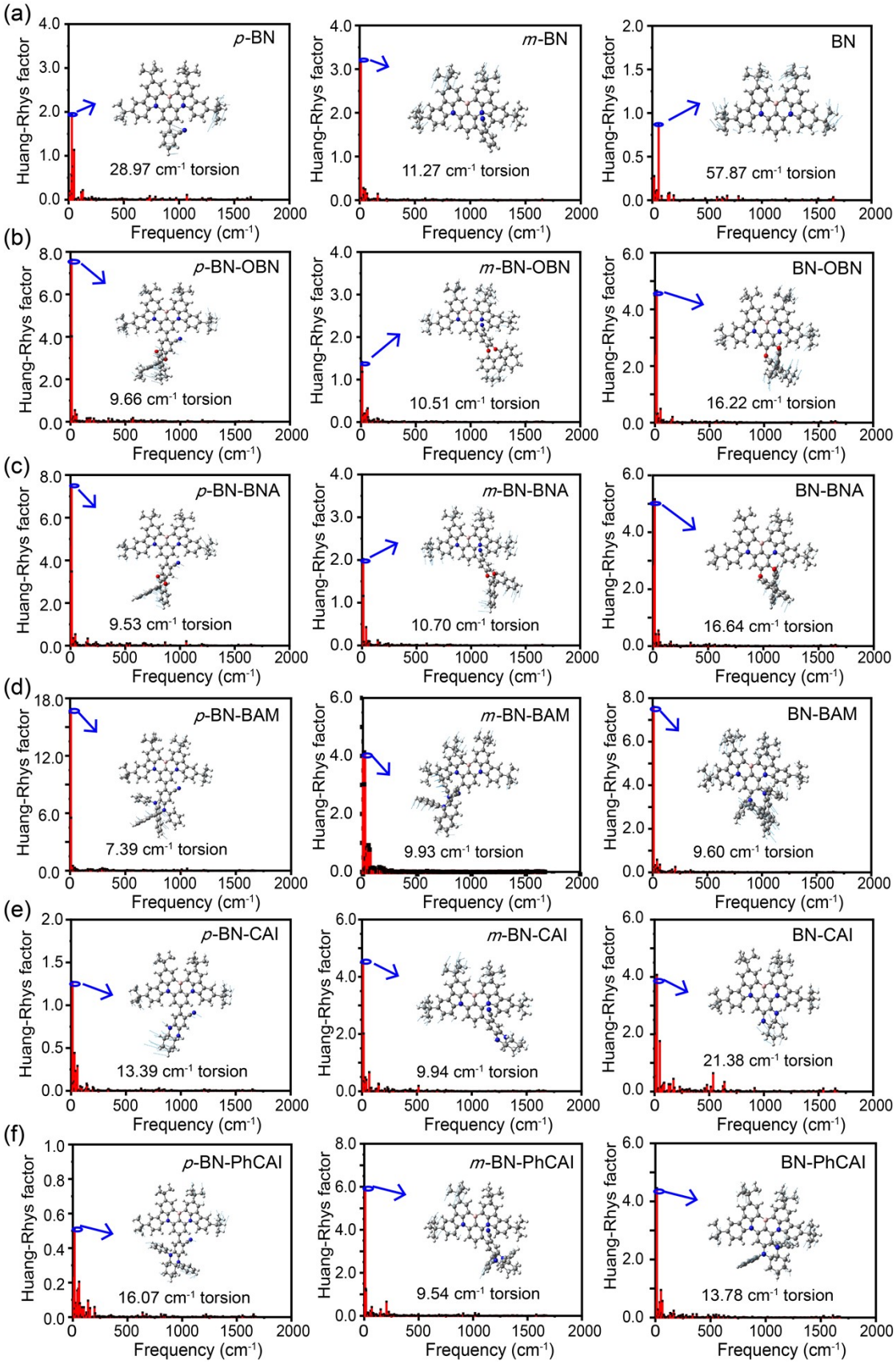

Figure S5. Calculated Huang-Rhys factors versus the normal mode frequencies for (a) the model, (b) OBN, (c) BNA, (d) BAM, (e) CAI and (f) PhCAI series molecules

where the representative vibration modes are shown as insets.

The transition of exciton from the ground state to the excited state through excitation or from excited state to ground state through emission can lead to geometric relaxation between S0 and S1. The recombination energy in the process of intramolecular structure relaxation can be calculated from the relevant points and equations on the adiabatic potential energy surface (PES).[1-3]

$\lambda_{S0} = E_0(ES) - E_0(GS)$

Here, E_0 (ES) is the energy of the S_0 state with the optimized S_1 geometry, E_0 (GS) is the energy of the S_0 state with the optimized S_0 geometry, E_1 (GS) is the energy of the S_1 state with the optimized S_0 geometry, E_1 (ES) is the energy of the S_1 state with the optimized S_1 geometry.

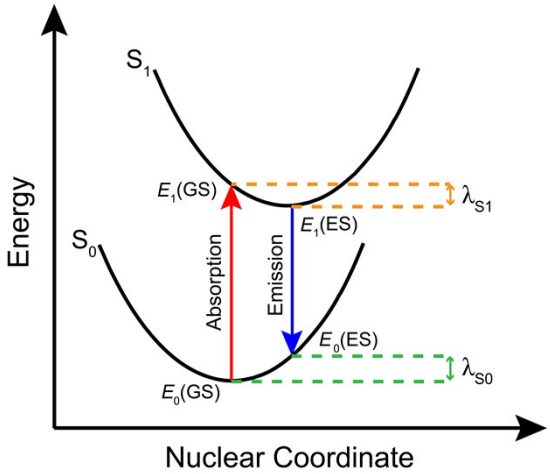

Figure S6. Sketch of the potential energy surfaces of S_0 and S_1.

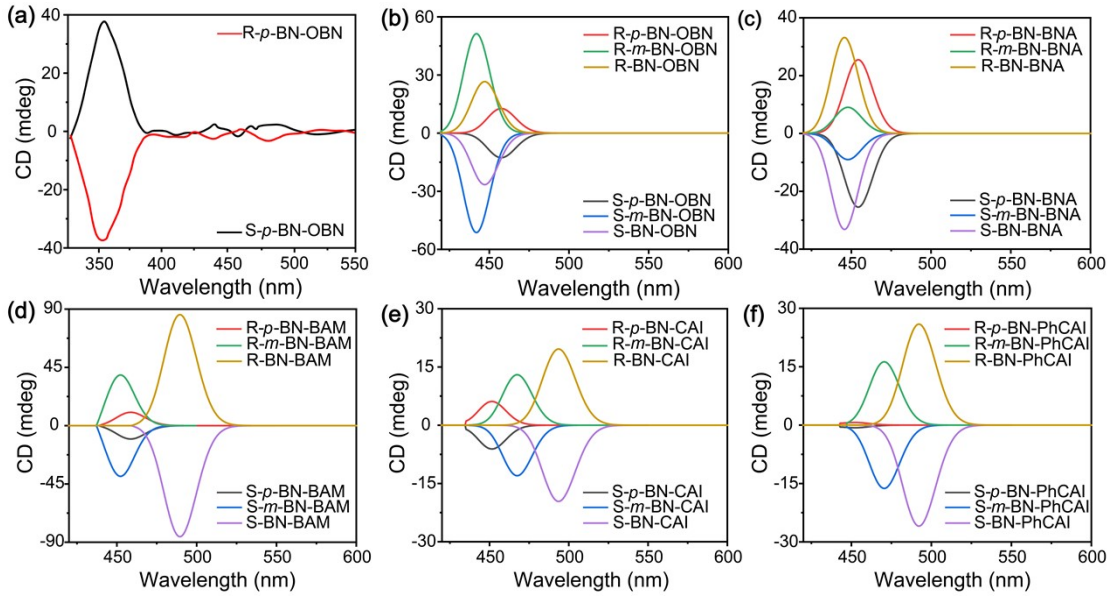

Figure S7. Experimental circular dichroic spectrum for (a) *p*-BN-OBN and simulated electronic circular dichroism spectra for (b) OBN, (c) BNA, (d) BAM, (e) CAI and (f) PhCAI series molecules.

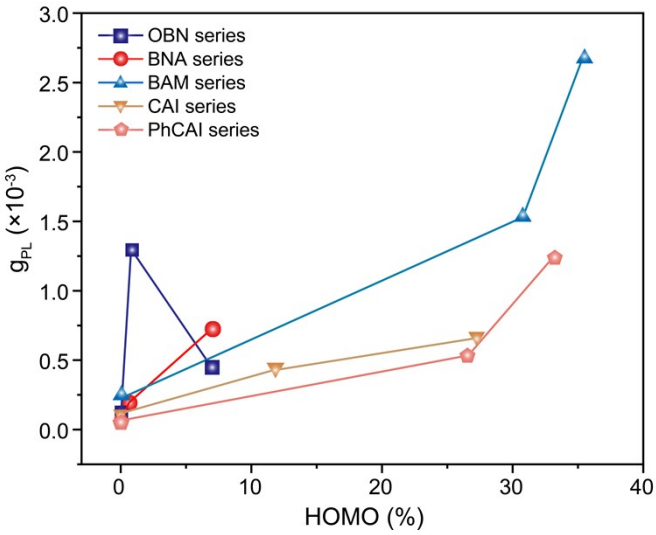

Figure S8. Changing trends between the chiral participations in HOMO composition and the g_{PL} values of different chiral series.

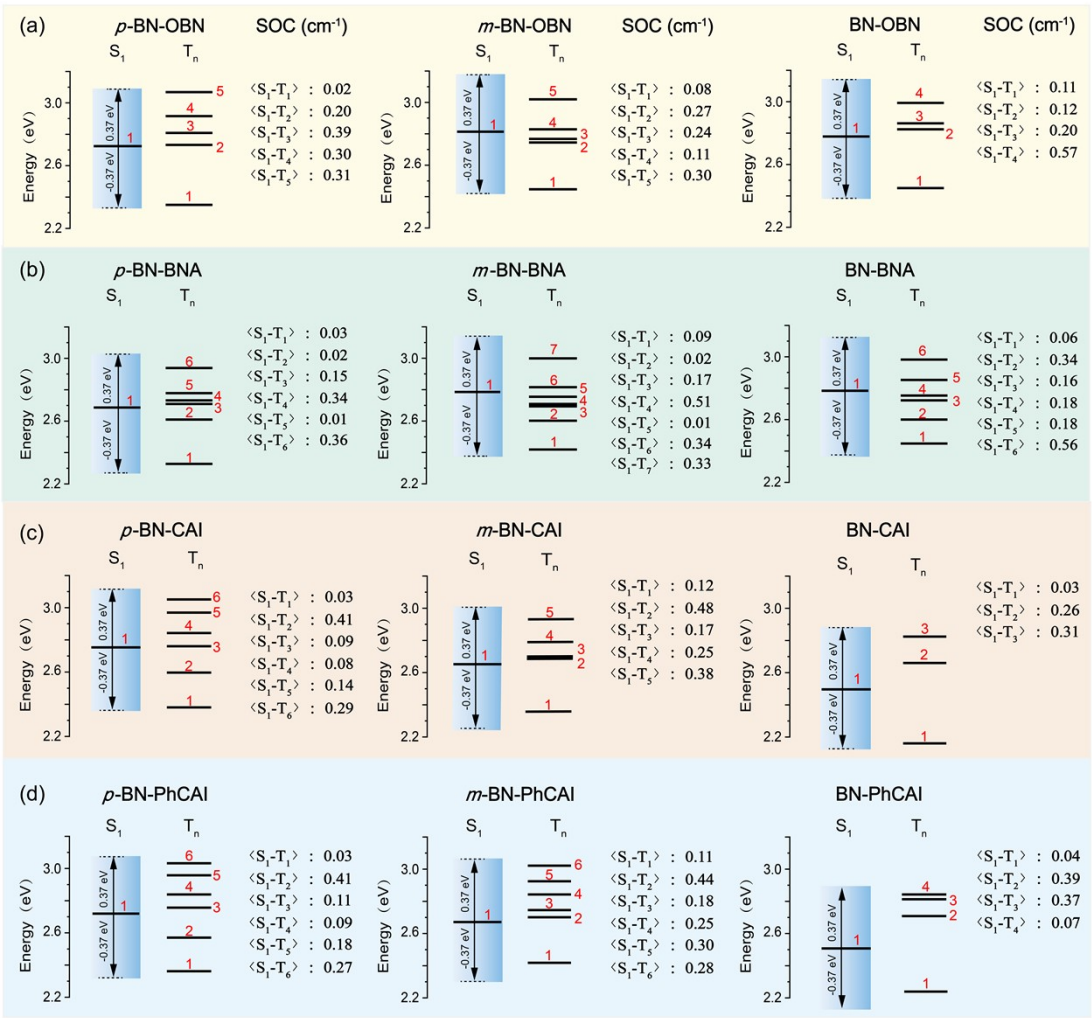

Figure S9. Calculated vertical excitation energies and the SOC constants between S_1 and T_n states for (a) OBN, (b) BNA, (c) CAI and (d) PhCAI series molecules in toluene.

Table S1. Absorption peak wavelength of *p*-BN-OBN predicted by different DFT functional.

Method classification	Computing method	HF (%)	λ_{abs} (nm)
Hybrid functional	O3LYP	11.6	491.20
	B3LYP	20	457.50
	PBE0	25	441.40
Long-range correction functional	CAM-B3LYP	19%-short-range 65%-long-range	385
Experimental	--	--	474

Table S2. Calculated the maximum absorption and emission wavelengths, transition characters, FWHM values (emission band at long wavelength) and reorganization energies (emission process) of the investigated molecules.

Compd.	Absorption properties		Emission properties			
	λ_{abs}（nm）	Transition characters（%）	λ_{PL}（nm）	Transition characters（%）	FWHM（nm/eV）	λ_{S0} (eV)
p-BN	460	H→L（98.78）	498	H→L（99.07）	24.5/0.122	0.18
m-BN	447	H→L（98.45）	467	H→L（98.57）	21.7/0.123	0.06
BN	443	H→L（98.82）	463	H→L（98.93）	21.0/0.121	0.07
p-BN-OBN	458	H→L（98.72）	488	H→L（98.94）	23.8/0.124	0.33
m-BN-OBN	442	H→L（98.42）	462	H→L（98.53）	23.1/0.131	0.07
BN-OBN	447	H→L（98.71）	486	H→L（98.97）	23.8/0.124	0.16
p-BN-BNA	459	H→L（98.73）	492	H→L（98.98）	24.0/0.123	0.34
m-BN-BNA	448	H→L（98.49）	468	H→L（98.61）	22.2/0.125	0.08
BN-BNA	446	H→L（98.60）	482	H→L（98.89）	23.4/0.125	0.16
p-BN-BAM	459	H→L（98.44）	489	H→L（98.74）	24.0/0.125	0.37
m-BN-BAM	452	H→L（89.10） H-1→L（8.54）	491	H→L（94.09） H-1→L（4.10）	24.0/0.123	0.14
BN-BAM	490	H→L（98.42）	538	H→L（98.87）	28.7/0.123	0.15
p-BN-CAI	452	H→L（98.67）	470	H→L（98.77）	22.4/0.125	0.07
m-BN-CAI	467	H→L（96.37） H-1→L（2.49）	529	H→L（98.05）	28.0/0.124	0.21
BN-CAI	494	H→L（98.52）	624	H→L（99.30）	38.0/0.121	0.39
p-BN-PhCAI	452	H→L（98.65）	471	H→L（98.75）	22.2/0.124	0.06
m-BN-PhCAI	471	H→L（95.06） H-1→L（3.84）	532	H→L（97.85）	28.7/0.126	0.30
BN-PhCAI	492	H→L（98.73）	590	H→L（99.22）	35.1/0.125	0.23

Table S3. Calculated percentage of different molecular segments in HOMO composition and the g_{PL} values.

Mol.	HOMO (%)		g_{PL}
	Chiral unit	MR core	
p-BN-OBN	0.01	99.99	9.16×10^{-5}
m-BN-OBN	0.79	99.21	1.30×10^{-3}
BN-OBN	6.95	93.05	4.50×10^{-4}
p-BN-BNA	0.01	99.99	7.10×10^{-5}
m-BN-BNA	0.65	99.35	1.95×10^{-4}
BN-BNA	6.64	93.36	6.98×10^{-4}
p-BN-BAM	0.06	99.94	2.27×10^{-4}
m-BN-BAM	30.78	69.22	1.53×10^{-3}

BN-BAM	35.41	64.59	2.69×10^{-3}
p-BN-CAI	0.01	99.99	1.17×10^{-4}
m-BN-CAI	11.57	88.43	4.25×10^{-4}
BN-CAI	27.21	72.79	6.59×10^{-4}
p-BN-PhCAI	0.01	99.99	6.51×10^{-5}
m-BN-PhCAI	26.61	73.39	5.34×10^{-4}
BN-PhCAI	33.18	66.82	1.25×10^{-3}

Table S4. Calculated oscillator strengths and radiation rates of the investigated molecules.

Compd.	f	k_r（s^{-1}）
p-BN	0.3400	3.40×10^{7}
m-BN	0.4362	7.20×10^{7}
BN	0.4621	1.26×10^{8}
p-BN-OBN	0.3837	2.03×10^{7}
m-BN-OBN	0.3928	6.64×10^{7}
BN-OBN	0.3456	4.11×10^{7}
p-BN-BNA	0.3640	2.21×10^{7}
m-BN-BNA	0.4365	5.20×10^{7}
BN-BNA	0.3509	4.25×10^{7}
p-BN-BAM	0.3404	8.20×10^{6}
m-BN-BAM	0.2441	2.49×10^{7}
BN-BAM	0.2036	1.44×10^{7}
p-BN-CAI	0.4443	8.99×10^{7}
m-BN-CAI	0.1795	1.61×10^{7}
BN-CAI	0.1474	6.24×10^{6}
p-BN-PhCAI	0.4278	7.12×10^{7}
m-BN-PhCAI	0.1555	4.69×10^{6}
BN-PhCAI	0.1447	1.05×10^{7}

Notes and references

1. Z.-P. Yan, T.-T. Liu, R. Wu, X. Liang, Z.-Q. Li, L. Zhou, Y.-X. Zheng and J.-L. Zuo, *Adv. Funct. Mater.*, 2021, **31**, 2103875.
2 X. Qiu, G. Tian, C. Lin, Y. Pan, X. Ye, B. Wang, D. Ma, D. Hu, Y. Luo and Y. Ma, *Adv. Opt. Mater.*, 2021, **9**, 2001845.
3. J. Li, F. Zhao, Y. Chen, M. Zhang, T. Li and H. Zhang, *J. Mater. Chem. C*, 2021, **9**, 15309-15320.